ACS OMEGA

http://pubs.acs.org/journal/acsodf

Article

# *In Vitro* Neuroprotective Effects of Macrophage Membrane-Derived Curcumin-Loaded Carriers against 1-Methyl-4-phenylpyridinium-Induced Neuronal Damage

Li-Ming Shen, Meng-Chu Li, Wen-Juan Wei, Xin Guan, and Jing Liu*

Cite This: *ACS Omega* 2021, 6, 32133−32141

Read Online

ACCESS | Metrics & More | Article Recommendations

**ABSTRACT:** Curcumin (CUR) possesses neuroprotective effects. However, its clinical therapeutic efficacy is limited because of its low systemic bioavailability due to poor water solubility and fast metabolism. Herein, we designed biomimetic therapeutic nanovesicles (NVs) with enhanced performance and biocompatibility for the intracellular delivery of hydrophobic CUR. Cell membrane NVs were constructed to function as drug carriers by the serial extrusion of macrophages using filters with decreasing pore sizes. Various CUR loading strategies were also evaluated. Furthermore, the neuroprotective effects of the CUR-loaded NVs (NVs−CUR) against 1-methyl-4-phenylpyridinium ($MPP^+$)-induced neuronal degeneration were studied thoroughly. CUR-loaded NVs were readily taken up by neurons *in vitro*, and the survival rate of $MPP^+$-induced primary neurons increased from 65.37 ± 6.37 to 90.91 ± 3.18% after pretreatment with NVs−CUR. Compared with traditional Parkinson's disease chemotherapeutic treatment, NV formulations can improve the bioavailability of this drug. NVs are expected to become a new and effective drug-delivery platform for further applications in the field of central nervous system therapy.

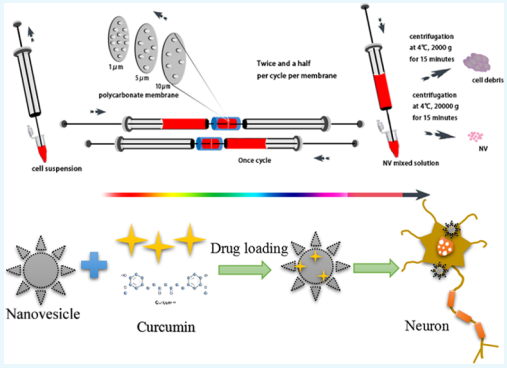


## INTRODUCTION

Parkinson's disease (PD) is a progressive degenerative disorder of the central nervous system, and its clinical pathology feature is the progressive loss of dopaminergic neurons in the substantia nigra. The neurotoxin 1-methyl-4-phenylpyridinium ($MPP^+$) acts selectively on dopaminergic neurons in the nigrostriatal system. Once $MPP^+$ is transferred into dopaminergic neurons with the assistance of a dopaminergic transporter, multienzyme complex I of the mitochondrial electron transport chain is inhibited. Then, the generation of reactive oxygen species increased, and intracellular oxidative stress increased.[1,2] $MPP^+$ induces a syndrome in cellular and animal models that closely resembles PD, that is, loss of nigrostriatal dopaminergic neurons. This further leads to a decrease in the concentration of dopamine and its biosynthetic enzyme tyrosine hydroxylase.[3] More importantly, $MPP^+$ causes $\alpha$-synuclein accumulation in the nigrostriatal dopaminergic neurons, which is also the main pathological feature of PD.[4] Therefore, $MPP^+$ is widely applied to construct *in vitro* models to test antiparkinsonian agents.

The main treatment regimen for PD is drug therapy targeting key molecular in pathological mechanism, including carbidopa/L-DOPA, DA agonists, and so forth.[5] However, most of these treatments can only alleviate the signs or symptoms of PD and improve the overall life quality of patients to a certain extent. In addition, current pharmacological treatments are associated with motor complications and side effects that are potentially disabling. As PD progresses, the dose of drugs needs to be increased to maintain sufficient therapeutic effects. Higher dose may cause more serious side effects. Currently, PD drug discovery has been confronted with two challenges: delivery of a sufficient dose of drug across the blood brain barrier to the lesion and a reduction in the side effects after repeated dosing.[6] Thus, researchers endeavor to increase drug availability,[7] and the development of nanosized drug formulation has a promising prospect.[8]

Curcumin (CUR), 1,7-bis(4-hydroxy-3-methoxyphenyl)-1,6-heptadiene-3,5-dione, is a natural polyphenol extracted from *Curcuma longa* Linn.[9] CUR exhibits multiple pharmacological activities, such as anti-inflammatory, antioxidant, and antiapoptotic properties.[10,11] Therefore, the potential of CUR to treat neurodegenerative diseases, autoimmune diseases, and cancer has attracted researchers' attention. Additionally, several

**Received:** September 5, 2021
**Accepted:** October 25, 2021
**Published:** November 16, 2021

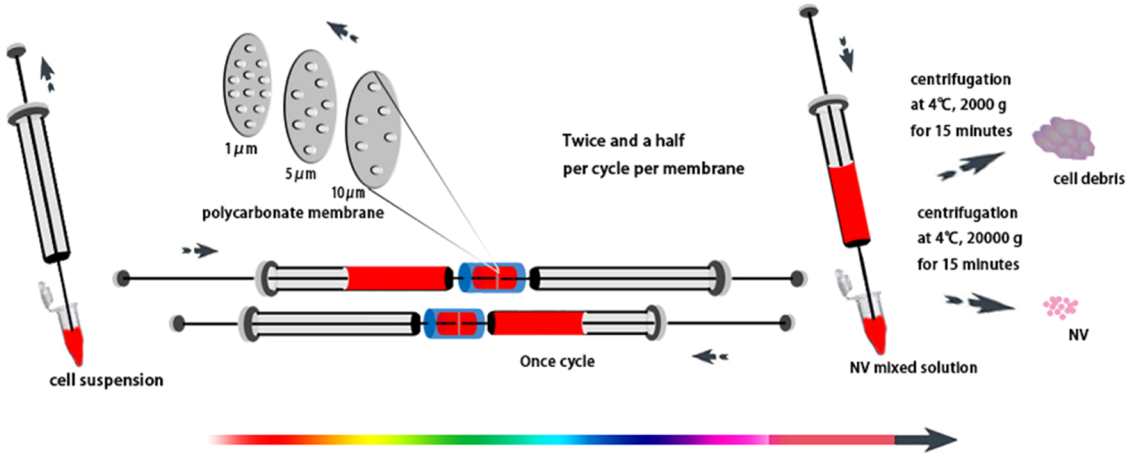


**Figure 1.** Schematic illustration of biomimetic NV preparation and purification. The RAW264.7 cell suspension was continuously extruded through a small extruder with three different-sized membranes five times to obtain a NV mixture. NV purification was performed by two-step centrifugation.

preclinical and clinical trials involving CUR are underway.[12] Despite its extensive research and development, the bioavailability of CUR through various routes of administration is low due to its poor water solubility and rapid metabolism and excretion, which limits its clinical therapeutic efficacy. Its water solubility is only 11 ng $mL^{-1}$ at pH 5.0. In addition, soluble CUR molecules are extremely unstable due to its rapid hydrolytic degradation. It has been reported that the maximum serum concentration of CUR can reach only 0.06 $\mu g$ $mL^{-1}$ even after its oral administration at a dose of 500 mg $kg^{-1}$, indicating only 1% oral bioavailability.[13] To circumvent these obstacles, conjugates of CUR with cyclodextrins[14] or DNA structures[15] or nanoformulations formed by encapsulating CUR into liposomes,[16] polymeric micelles,[17] nanogels,[18] or nanoparticles, and so forth[19,20] have been investigated to enhance its water solubility, thereby increasing its circulation time and bioavailability. Rakotoarisoa proved that the encapsulation of CUR into nanoparticles enhanced their neuroprotective potential against oxidative stress in a neurodegenerative disorder model.[21,22]

The aforementioned nanoformulations are often composed of inorganic or organic synthetic materials. In practice, these exogenous nanoformulations usually encounter opsonization and nonspecific clearance by the reticuloendothelial system.[23] PEGylation was usually applied to camouflage the carrier to circumulate a nonspecific rejection problem. Even so, the human complement system could be inevitably activated and eliminate the drug.[24] Therefore, the exploration of biomimetic strategies to transport CUR has sparked extensive research interest. Extracellular vesicles (EVs) are typically lipid−(glyco)protein membrane-enclosed vesicular structures, with proteins and nucleic acids derived from the parent cell encapsulated in the hydrophilic core. In view of EVs' biogenesis, they carry parental cell information and possess the natural properties of the parent cells. EVs have shown great potential for drug delivery owing to their amphiphilic property and endogenous origin.[25−28] However, spontaneously generated EVs suffer from low production yield, heterogeneity in size and composition, and inefficient drug packaging. Homogeneous biomimetic nanovesicles (NVs) can be fabricated by subjecting cells to serial extrusion through successively diminishing pore sizes. As previously reported, this approach can promote a production yield that is up to 100-fold higher than that obtained through spontaneous processes.[29] Overall, NVs combine the advantages of both man-made nanocarriers and EVs while breaking through their defects. Furthermore, NVs are immune privileged compared to PEGylated nanoformulations, which will avoid being eliminated by the organism. Herein, we successfully associated CUR with NVs derived from macrophages and performed an initial assessment of their protective effects on $MPP^+$-damaged neurons.

## RESULTS AND DISCUSSION

**Construction and Characterization of the NVs.** As a major immune regulator, macrophages not only possess long blood circulation time but also carry many recognition receptors on their membranes to discern inflammation and diseased regions.[30−32] Therefore, macrophage membrane-derived NVs could be a potential biomimetic drug-delivery carrier to avoid clearance by the mononuclear phagocyte system, overcome the biological barrier, and target the lesion in a sufficient quantity. RAW264.7 single-cell suspensions were collected and continuously extruded through a series of successively diminishing pore sized polycarbonate (PC) membranes (Figure 1). After several extrusions, the solution changed from turbid to transparent. The resulting mixture was subsequently purified by two-step centrifugation and resuspended in sterile phosphate-buffered saline (PBS) for storage at −80 °C prior to use. Transmission electron microscopy (TEM) characterization indicated that the NVs were enclosed vesicles. Cellular debris and protein aggregates were absent in the TEM images (Figure 2A). The morphology of NVs displayed a cup-shaped appearance similar to exosomes.[33] According to the TEM images, the NVs prepared by continuous extrusion through a single-sized PC membrane were approximately 165.3 nm in diameter (method I), while the average diameter of the NVs prepared from sequential extrusion through different-sized PC membranes (method II) was approximately 54.8 nm. In addition, the NVs produced by method I showed remarkable agglomeration. The height and particle sizes of the NVs were also evaluated by atomic force microscopy (AFM). The average height of the NVs was 14 nm, and the average particle size was approximately 90 nm (Figure 2B,C). Dynamic light scattering (DLS) analysis of NVs revealed a hydrodynamic size distribution with peak diameters of 385.6 and 123.2 nm for method I and method II, respectively (Figure 2D). Based on the comprehensive analysis,


https://doi.org/10.1021/acsomega.1c04894
ACS Omega 2021, 6, 32133−32141

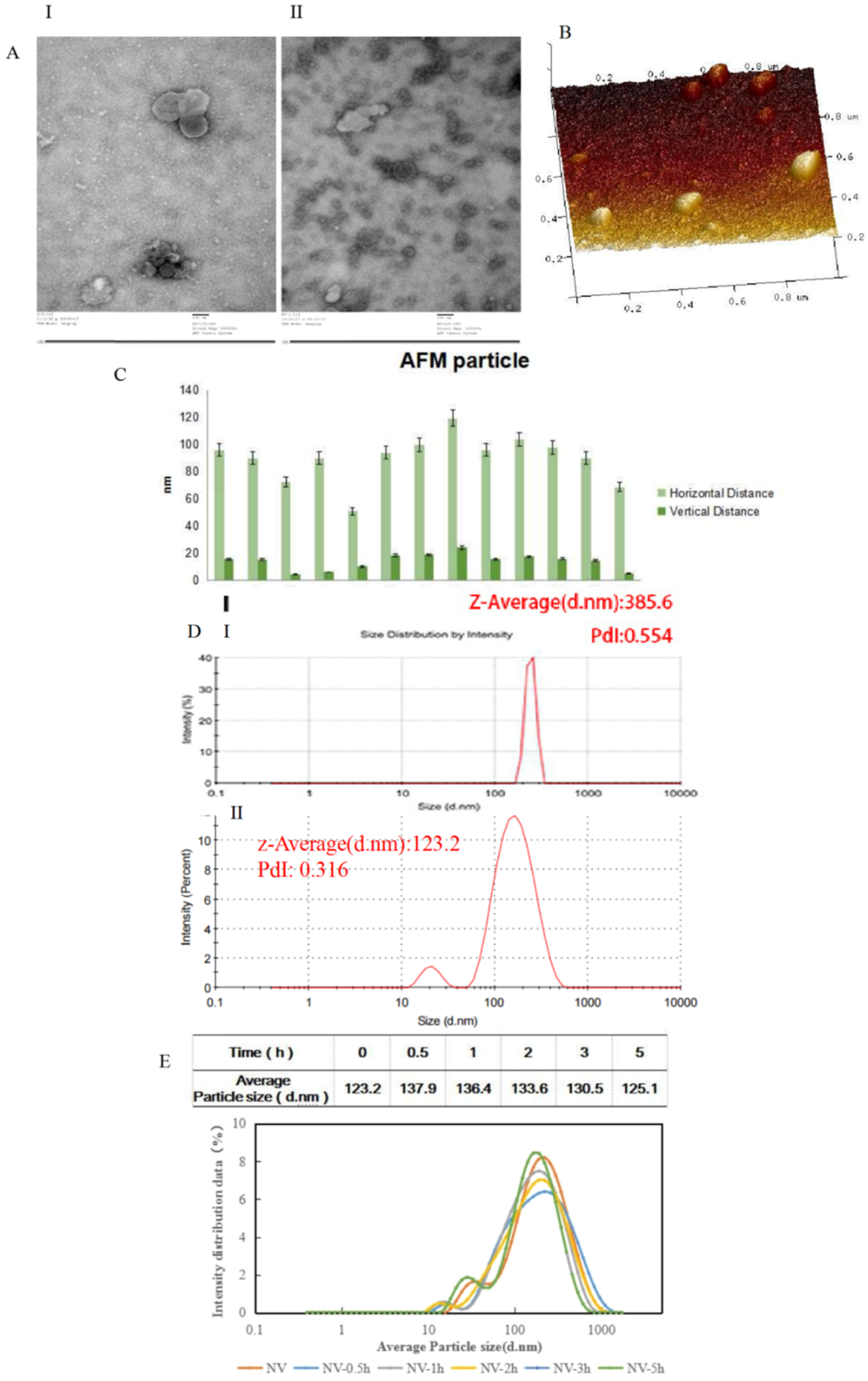


**Figure 2.** Characterization of the RAW264.7-derived NVs. (A) TEM images of the NVs prepared by method I and method II (scale bar, 100 nm). (B) AFM images of the NVs prepared by method I. (C) Height analysis of NV from AFM data. (D) Hydrodynamic sizes of the NVs prepared by method I and method II. (E) Hydrodynamic size of the NV in PBS after 5 h.

method II produced more homogeneous and well-dispersed NVs with low polydispersity. Therefore, NVs prepared by method II were used for subsequent experiments. It has been noted that nanomaterials ranging in size from 5 to 200 nm are suitable as drug vehicles because nanoparticles smaller than 5 nm were rapidly excreted through the kidneys, while nanoparticles larger than 200 nm were usually enriched in the spleen, liver, and lungs.[34] Overall, these NVs are ideal


https://doi.org/10.1021/acsomega.1c04894
ACS Omega 2021, 6, 32133−32141

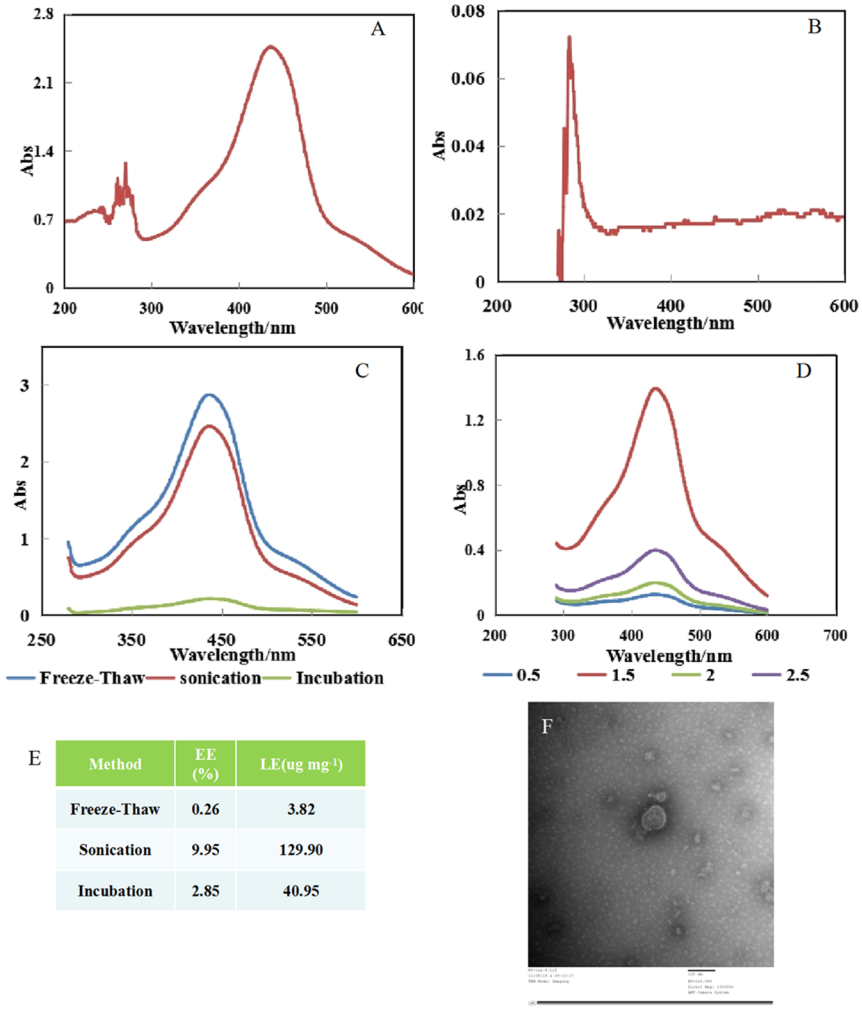


E

| Method | EE (%) | LE(ug mg$^{-1}$) |
|---|---|---|
| Freeze-Thaw | 0.26 | 3.82 |
| Sonication | 9.95 | 129.90 |
| Incubation | 2.85 | 40.95 |




**Figure 3.** Preparation and efficiency of the NVs−CUR. UV−vis spectrum of CUR (A) and NVs (B). (C) UV−vis spectra of the NVs−CUR prepared by means of freeze−thaw cycles, sonication, and incubation at RT. The amount of CUR added was 1.5 mg. (D) UV−vis spectra of the NVs−CUR constructed by sonication of the NVs with a series of concentrations of CUR. (E) Comparison of the EE and drug LE after the three drug incorporation modes. (F) NV−CUR morphology examined by TEM.

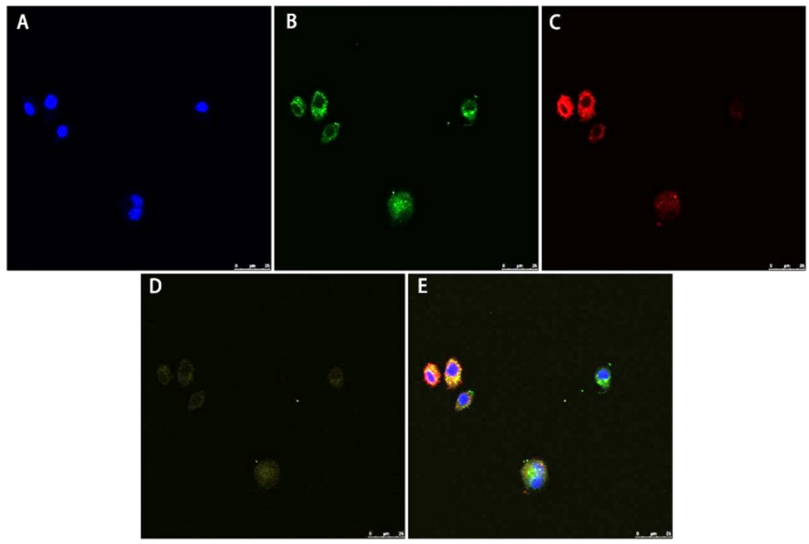


**Figure 4.** Cellular uptake and intracellular localization of the NVs−CUR in RAW264.7 cells by fluorescence confocal microscopy. (A) RAW264.7 nuclei were stained with DAPI. (B) RAW264.7 cell membrane was stained with DiO (green). (C) NVs were stained with DiD (red). (D) Yellow represents the CUR located in the cytoplasm. (E) Overlay of the cells and the NVs−CUR. The scale bar is 25 $\mu$m.



https://doi.org/10.1021/acsomega.1c04894
*ACS Omega* 2021, 6, 32133−32141

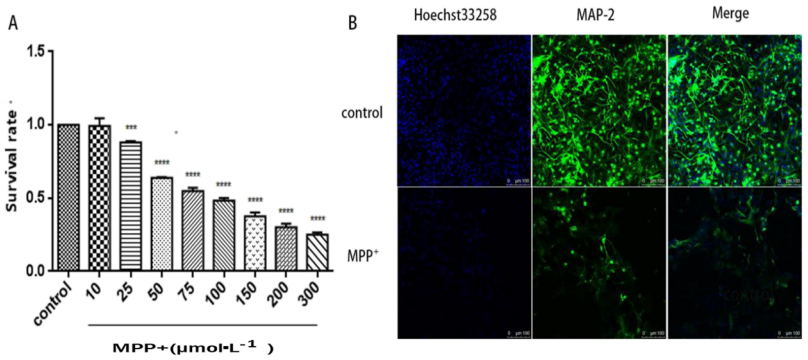


**Figure 5.** Effects and morphological changes after $MPP^+$ treatment in primary mesencephalic neurons. (A) Damaging effects of different concentrations of $MPP^+$ on rat primary neurons. ***$P < 0.001$, ****$P < 0.0001$ *vs* the control. (B) Morphology of 7 day primary neurons after treatment with 100 $\mu$mol $L^{-1}$ $MPP^+$ for 48 h as observed by laser confocal microscopy. The scale bar is 100 $\mu$m.

candidate carriers for drug delivery. By method II, the preparation of NVs takes approximately 20 min, and the two-step purification takes 30 min. The whole procedure takes less than 1 h. DLS was performed at 0, 0.5, 1, 2, 3, and 5 h to test the stability of the NVs. The average particle sizes of the NVs in PBS were 123.2, 137.9, 136.4, 133.6, 130.5, and 125.1 nm at these times. The hydrodynamic size change of the NVs were within the normal range, indicating that these NVs were stable during storage (Figure 2E).

**Efficiency of Loading CUR into the NVs.** Three different protocols for incorporating CUR into NVs were explored. As depicted in Figure 3A,B, the ultraviolet−visible (UV−vis) spectrum of CUR showed a main band centered at 436 nm, and the band of the NV did not interfere with that of CUR. The drug loading efficiency (LE) was determined by the UV−vis absorbance spectra, and the amounts of loaded CUR in the NVs−CUR were estimated to be 129.90, 40.95, and 3.82 $\mu$g $mg^{-1}$ for the sonication, incubation, and freeze−thaw methods, respectively. Correspondingly, the encapsulation efficiency (EE) values of CUR in the NVs were 9.95, 2.85, and 0.26% (Figure 3E). Thus, the UV−vis spectroscopy results of the NV−CUR complexes demonstrated that sonication was the optimum drug incorporation method (Figure 3C). These data indicate that the loading capacity (LC) of the NV−CUR formulations strongly relied on the preparation method. Hereafter, sonication was applied to efficiently load the drug into the NVs. We speculated that the cavitation or sonication effects produced by ultrasound caused the NVs to produce instantaneous repairable membrane voids, thereby greatly increasing the chance of drug entry into the NVs.[35] We also optimized the initial input amount of CUR for drug loading by examining 0.5, 1.5, 2.0, and 2.5 mg (Figure 3D). The results showed that the maximum absorption peak from the NVs−CUR was obtained with 1.5 mg of CUR input. Furthermore, we investigated the morphology of the NVs−CUR fabricated by sonication, and it was similar to that of the NVs with regular morphology, indicating the stability of this drug-loaded NV structure (Figure 3F).

**Cellular Uptake Studies.** To examine the interaction between the NVs−CUR and cells, drug-loaded NVs and RAW264.7 cells were incubated at 37 °C for 1.5 h. The cellular uptake efficiency was determined by confocal microscopy. As shown in Figure 4C, the NVs−CUR exhibited significant cell uptake behavior and accumulated in the cytoplasm. Moreover, the yellow fluorescence in the cells illustrated that the CUR encapsulated in the NVs was also located in the cytoplasm, confirming that these NVs could function as drug carriers to transfer CUR into cells. Since the whole preparation process of the macrophage cell membrane vesicles maintains the lipid bilayer structure and minimizes the damage to the membrane-bound proteins, these NVs should inherit the biological functions of the parent cells after translocation. As cell-derived membrane vesicles, NVs were prone to interact with recipient cells, which could facilitate internalization by cells. In this respect, this novel drug carrier based on fusion after cell membrane disruption greatly reduces toxicity and immunogenicity compared with existing synthetic nanodrug carriers. Further, as a membrane structure carrier, these NVs can fuse with the target cell membrane, thereby directly delivering its encapsulated drug to the recipient cells, increasing the drug delivery efficiency, and avoiding the cytotoxicity produced by the endocytic-lysosomal pathway.[36]

**Effects of $MPP^+$ on Primary Mesencephalic Neurons.** *In vitro* PD models are essential for drug evaluation and screening during drug development. The most commonly used cell lines include human neuroblastoma cells (SH-SY5Y), immortalized human dopaminergic neuron precursor cells (LUHMES), rat adrenal pheochromocytoma cells (PC12), and mouse midbrain dopaminergic neuron cells (MN9D).[37] In this study, we used Sprague-Dawley (SD) rat primary neurons to construct an *in vitro* PD model since they not only highly resemble the morphology and physiology of neuronal cells but also express the essential proteins. To select the appropriate toxin dose, different concentrations of $MPP^+$ (10−300 $\mu$mol $L^{-1}$) were used to treat 7 day neurons for 48 h, and then the effects of $MPP^+$ on the survival rate of the primary mesencephalic neurons were measured by the CCK8 method. As the concentration of $MPP^+$ increased, the viability of the neurons gradually decreased (Figure 5A). In subsequent experiments, we used 100 $\mu$mol $L^{-1}$ $MPP^+$ to induce neurological damage, and the $MPP^+$-induced neurotoxicity in mesencephalic neurons was evaluated by an immunofluorescence assay. Under a confocal microscope, the positive expression of MAP2 in the primary neurons was observed and the synaptic growth was in good state; notably, the synapses between neurons were connected to form a dense neural network with a stereoscopic effect (Figure 5B). However, after incubation with 100 $\mu$mol $L^{-1}$ $MPP^+$ for 48 h, the number of neurons decreased significantly, the synaptic connections between neurons were significantly reduced, and most of the synapses were discontinuous; only approximately 50% of the remaining neurons were normal.


https://doi.org/10.1021/acsomega.1c04894
*ACS Omega* 2021, 6, 32133−32141

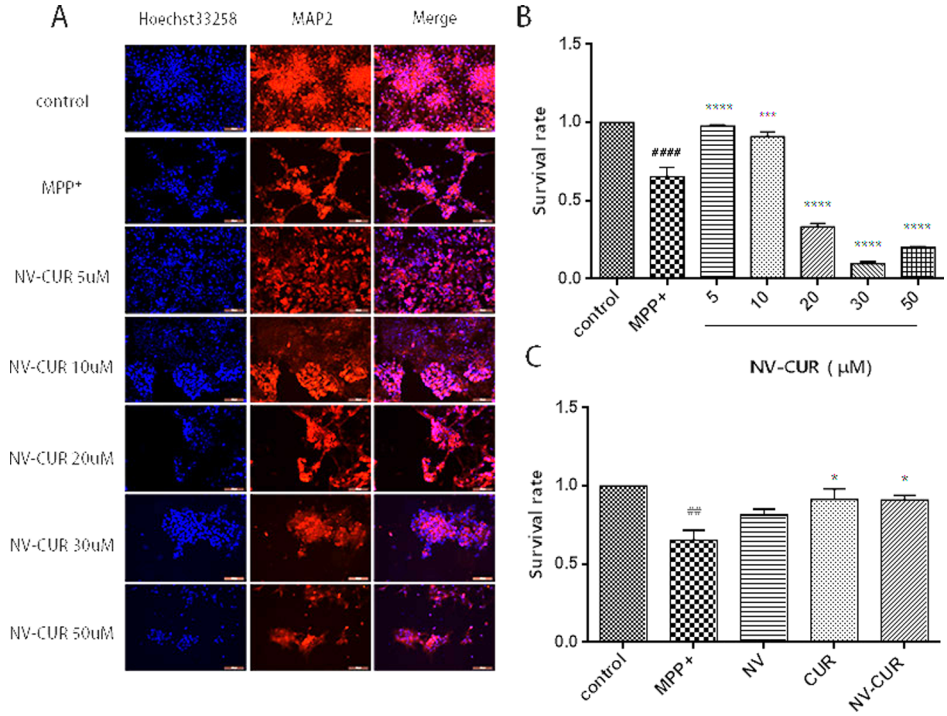


**Figure 6.** CUR-loaded NVs protect primary mesencephalic neurons from $MPP^+$-induced neuronal damage. Different concentrations of NVs−CUR interfered with $MPP^+$-induced primary neuron survival. (A) Observations by inverted fluorescence microscopy. Scale bar: 100 $\mu$m. (B) Survival rate calculated by the CCK8 assay. $^{\#\#\#\#}P < 0.0001$ *vs* the control; $^{***}P < 0.001$, $^{****}P < 0.0001$ *vs* $MPP^+$. (C) NVs−CUR (10 $\mu$mol $L^{-1}$) and the same masses of NV and CUR acting on $MPP^+$-induced primary neurons. $^{\#\#}P < 0.01$ *vs* the control; $^{*}P < 0.05$ *vs* $MPP^+$.

**Drug-Loaded NVs Protect Primary Mesencephalic Neurons from $MPP^+$-Induced Neuronal Damage.** We next evaluated the protective effects of different concentrations of NVs−CUR on the primary neurons. A series of concentrations of NVs−CUR (5, 10, 20, 30, and 50 $\mu$mol $L^{-1}$) were incubated with neurons for 2 h, and then $MPP^+$ was added for 48 h of incubation as described above. Under an inverted fluorescence microscope, there was an abundant number of neurons in the control group (without drug intervention), and the synapses were connected to form a neural network. The number of neurons in the $MPP^+$ group was significantly reduced, with nearly half surviving. However, the number of neurons in the 5 and 10 $\mu$mol $L^{-1}$ NV−CUR groups was significantly higher than that in the $MPP^+$ group, and these values were close to that of the control group. In contrast, the number of neurons in the high-concentration NV−CUR group decreased, and the synapses were discontinuous (Figure 6A). With increasing NV−CUR concentration, the protective effects gradually decreased along with the survival rate of the neurons, eventually showing a survival rate that was lower than that of the control group without drug intervention. Exposure of mesencephalic neurons to 100 $\mu$mol $L^{-1}$ $MPP^+$ induced a decrease in cell viability. NV−CUR treatment increased neuronal viability and substantially alleviated $MPP^+$-induced neuronal death. These results showed that the viability of neurons in the low-concentration NV−CUR group was significantly better than that in the high-concentration NV−CUR group. CUR has been shown to have concentration-dependent pleiotropic effects on cells; low CUR concentrations protect neurons, but higher concentrations are neurotoxic. Sun claimed that CUR complexed with RAW264.7-derived exosomes can be absorbed into activated monocyte-derived myeloid cells and then CUR induced apoptosis of monocytes subsequently.[38] Compared with the $MPP^+$ group, the survival rates of the neurons in the 5 and 10 $\mu$mol $L^{-1}$ NV−CUR groups markedly increased ($P < 0.001$, $P < 0.0001$); specifically, the survival rate of the neurons in the $MPP^+$ group was 65.37 ± 6.37% and those in the 5 and 10 $\mu$mol $L^{-1}$ NV−CUR groups reached 97.85 ± 0.77 and 90.91 ± 3.18%, respectively (Figure 6B).

Although the number of neurons in the 5 $\mu$mol $L^{-1}$ NV−CUR group was closer to that in the control group than in the 10 $\mu$mol $L^{-1}$ NV−CUR group, the state of neurons in the 5 $\mu$mol $L^{-1}$ NV−CUR group was not as good as that in the 10 $\mu$mol $L^{-1}$ NV−CUR group. Therefore, subsequent experiments to further study the protective effects on neurons used 10 $\mu$mol $L^{-1}$ NVs−CUR. In addition, we evaluated the protective effects of the NVs, CUR, and NVs−CUR on neurons. Compared with the $MPP^+$ group, the increase in the neuronal survival rate in the NV group was not significant ($P > 0.05$), indicating that the NVs have neither toxic nor protective effects on neurons. Notably, compared with the $MPP^+$ group, the survival rates of the neurons in the CUR and NV−CUR groups significantly increased (Figure 6C) to 91.26 ± 6.88 and 90.91 ± 3.18%, respectively.

The key finding of our study is that the specific NV−CUR formulation significantly increased neuronal survival in a neuronal damaged model. Previous studies have shown that CUR has anti-inflammatory properties, antioxidative effects, and a potential protective influence on nigrostriatal dopaminergic neurons.[22] In this study, hydrophobic CUR was encapsulated in macrophage-derived NVs. Because NV membrane carried multiple adhesive proteins from parent cells, NVs can interact with target cells through surface proteins and vector ligands (tetraspanins) and are then taken


https://doi.org/10.1021/acsomega.1c04894
ACS Omega 2021, 6, 32133−32141

up by target cells to successfully deliver their payload in the end.[39]

## CONCLUSIONS

In summary, we successfully constructed nanoformulations made of biomimetic cell membrane NVs and an antioxidant drug through a top-down assembly that acts as a biomimetic drug-delivery platform. These NVs were generated by the mechanical extrusion of macrophages. Afterward, the NV and CUR mixture was sonicated to facilitate CUR entry into the NVs. This drug-delivery system can be prepared in approximately 1 h. NVs−CUR exhibited neuroprotective efficacy against $MPP^+$-induced primary mesencephalic neuronal damage, and the activities are dose-dependent, that is, low CUR concentrations protect neurons, but higher concentrations are neurotoxic. Overall, this proof-of-concept study may offer a rapid and economic approach for the assembly of hydrophobic drugs into bioactive cellular NVs to improve the therapeutic efficacy of drugs in $MPP^+$-induced damage in cultured primary neurons, which could also be expanded to other biomedical applications.

## MATERIALS AND METHODS

**Cell Culture.** RAW264.7 cells were purchased from the National Collection of Authenticated Cell Cultures, China. The cells were grown in Dulbecco's modified Eagle's medium (DMEM) supplemented with 10% fetal bovine serum (FBS) and 1% penicillin/streptomycin at 37 °C in a humidified atmosphere of 5% $CO_2$. Cell culture reagents were purchased from Thermo Fisher. When the cells were cultured to appropriate confluence, adherent cells were detached with a cell scraper. Approximately, $1 \times 10^7$ cells were harvested and centrifuged. Pellets were dispersed into single-cell suspensions in PBS for subsequent NV preparation.

**Preparation of NVs.** Cell suspensions were continuously extruded 11 times *via* a 100 nm pore-sized PC membrane filter (Whatman, UK) using a miniextruder (Avanti Polar Lipids, USA) (method I). Alternatively, cell suspensions were sequentially extruded 5 times successively through 10, 5, and 1 $\mu$m PC membranes using a miniextruder (method II). For method I, after removing the cell debris by centrifugation at 2000*g* for 15 min at 4 °C, the supernatant collected was then subjected to centrifugation at 100 000*g* for 1 h at 4 °C. For method II, two-step centrifugation was performed at 2000*g* and 20 000*g* for 15 min each at 4 °C. Then, the pellet was dispersed in sterile PBS. The procedures for the preparation and isolation of the NVs are depicted in Figure 1.

**CUR Encapsulation into NVs.** CUR was obtained from Sinopharm Chemical Reagent Co., Ltd. (Shanghai, China). A 30 mg $mL^{-1}$ CUR stock solution was prepared in dimethyl sulfoxide (DMSO). Different concentrations of CUR (0.14, 0.42, 0.56, and 0.69 mg $mL^{-1}$) in PBS and DMSO mixture (v/v 2:1) were added to 0.28 $\mu g\ \mu L^{-1}$ NVs. Three approaches for encapsulating CUR into the NVs were evaluated: method I: freeze−thaw cycles; method II: sonication; method III: incubation at RT. In method I, the CUR solution was mixed with the NVs, incubated for 30 min, quickly frozen for 8 min at −80 °C, and then thawed at RT. This freeze−thaw cycle was repeated 3 times. In method II, the drug and NV mixture was sonicated for 15 min (2 kHz, 70% power) (KQ-600 KDE, Kunshan Ultrasonic Instruments Co., Ltd., China), cooled for 5 min at −20 °C, and then sonicated again. For method III, the drug and NV mixture was incubated at RT for 2 h. Two-step gradient centrifugation was performed to purify the NVs−CUR. The mixture was first centrifuged at 8000*g* for 15 min at 4 °C to separate the unloaded CUR, followed by centrifugation at 20 000*g* for 15 min at 4 °C. The yellowish brown precipitate was NVs−CUR and was resuspended in PBS.

**Characterization and Stability Analysis of the NVs.** The purified NVs−CUR and NVs (1 $\mu$L containing 1.21 $\mu$g of total protein) were dropped onto copper grids after fixation with an equal volume of 4% paraformaldehyde for 30 min at RT. The dried grids containing NVs−CUR or NVs were negative stained with phosphotungstic acid and then visualized using TEM (JEM-2000EX, JEOL, Japan). The three-dimensional morphologies of the NV surfaces were recorded by AFM (Dimension Icon, Bruker, Germany). A drop of NV suspension was put on a glass slide and blew to dry under a stream of argon. Afterward, the obtained images were analyzed using NanoScope Analysis software. The NV particle sizes and distribution were measured by DLS (Nano-ZS90, Malvern Zetasizer, UK). The stabilities of the NV were monitored by DLS at 0.5, 1, 2, 3, and 5 h.

**Determination of the Drug-Loading Efficiency.** To quantitatively determine the amount of incorporated CUR, purified NVs−CUR were collected, and the absorbance of CUR at 436 nm was measured with a UV−vis spectrometer (U-3900, HITACHI, Japan). The corresponding concentration of CUR in each NV−CUR sample was then calculated according to the calibration curve of CUR. Afterward, the drug EE (%) of NVs and LC were calculated according to the following equations:

$$\mathrm{EE} = \frac{C_{\mathrm{NVs-CUR}}}{C_{\mathrm{initial}}} \times 100\%$$

$$\mathrm{LC} = \frac{C_{\mathrm{NVs-CUR}}}{C_{\mathrm{NVs-CUR}} + N_{\mathrm{NVs}}}$$

where $C_{\mathrm{NVs-CUR}}$ is the amount of CUR in the NVs−CUR, $C_{\mathrm{initial}}$ is the initial amount of CUR added to the formulation, and $N_{\mathrm{NVs}}$ is the amount of NVs.

**Drug-Loaded NVs Uptake by RAW264.7 Cells.** To assess the uptake of the NVs−CUR by cells, RAW264.7 cells were seeded in 24-well plates (2000 cells/well). When the cells were completely adherent, 10 $\mu$mol $L^{-1}$ DiO green membrane dye was added followed by incubation for 20 min and three washes with PBS, each time for 5 min. Additionally, the NVs−CUR were incubated with 10 $\mu$mol $L^{-1}$ DiD red membrane dye for 20 min. Subsequently, the DiD-stained NVs−CUR were mixed with the cells for culture at 37 °C for 1.5 h. After incubation, the cells were incubated with 4% paraformaldehyde for 15 min and then incubated with DAPI for 7 min; after each step, the cells were washed three times with PBS, each time for 5 min. Cell uptake was determined by using a laser confocal microscope (Leica TCS SP8, Germany).

**$MPP^+$-Induced Damage to Primary Newborn Rat Mesencephalic Neurons.** All experiments involving animals were approved by the Dalian Medical University Institutional Animal Care and Use Committee. SD rats were obtained from the Institute of Genome Engineered Animal Models for Human Disease. The mice were bred in a specific pathogen-free facility at the Dalian Medical University. Primary mesencephalic neurons were isolated from 24 h-old newborn SD rats. Briefly, the midbrain neurons were carefully and gently


https://doi.org/10.1021/acsomega.1c04894
ACS Omega 2021, 6, 32133−32141

dissociated, extracted, and seeded onto poly-D-lysine-precoated 24-well or 96-well plates in cell culture medium composed of DMEM, nutrient F12, 10% FBS, 10% horse serum, 1% glutamine, and penicillin/streptomycin (DMEM/F12). Four hours later, the DMEM/F12 medium was discarded, and fresh Neurobasal-A medium supplemented with 2% B27, 1% glutamine, and penicillin/streptomycin were added to maintain homogeneous neuronal cell populations. Neurons cultured to day 7 were treated with a series of concentrations of $MPP^+$ (10, 25, 50, 75, 100, 150, 200, and 300 $\mu$mol $L^{-1}$) at 37 °C for 48 h.

**Cell Viability Assay.** Neuronal protection provided by NVs−CUR was assessed by the CCK8 assay. For this purpose, primary neurons were seeded into a 96-well plate and cultured for 7 days to allow neuronal maturation. Then, the neurons were exposed to 5, 10, 20, 30, or 50 $\mu$mol $L^{-1}$ NVs−CUR, free CUR, or empty NVs for 2 h. Subsequently, cell damage was induced by 100 $\mu$mol $L^{-1}$ $MPP^+$ for 48 h. Following incubation, the cells were rinsed with PBS. Then, 100 $\mu$L of neurobasal-A medium containing 10 $\mu$L of CCK8 was put into each well. After incubation at 37 °C for 1.5 h, the absorbance was detected at 450 nm using a microplate reader (EL808, BioTek, USA).

**Immunofluorescence Staining.** Neurons were fixed with 4% paraformaldehyde for 0.5 h, pretreated with 0.3% Triton X-100 for 20 min, and then incubated with anti-mouse tubulin-associated 2 (MAP2) polyclonal antibody (Abcam, 1:1000) overnight. Afterward, the cells were incubated with fluorescein isothiocyanate-conjugated fluorescent secondary antibodies (Abcam, 1:200) for 1 h, followed by incubation with Hoechst 33258 (Sigma, 1:1000) for 5 min. The entire staining operation was performed in the dark. After each step, the cells were rinsed three times with PBS, each time for 5 min. Confocal images were collected by laser confocal microscopy and inverted fluorescence microscopy with excitation wavelengths at 405 and 488 nm, respectively.

**Statistical Analysis.** Statistical analysis of data was performed with GraphPad Prism 6.0 software (GraphPad software). All values are expressed as the mean ± standard error of the mean. *P*-values were calculated using one-way analysis of variance, and a value of $P < 0.05$ was supposed to be significant.

## AUTHOR INFORMATION


### Corresponding Author

**Jing Liu** − *Stem Cell Clinical Research Center, The First Affiliated Hospital of Dalian Medical University, Dalian 116011, China; Dalian Innovation Institute of Stem Cell and Precision Medicine, Dalian 116023, China*; Email: liujing.dlrmc@hotmail.com

### Authors

**Li-Ming Shen** − *Stem Cell Clinical Research Center, The First Affiliated Hospital of Dalian Medical University, Dalian 116011, China*; orcid.org/0000-0002-5830-714X

**Meng-Chu Li** − *Stem Cell Clinical Research Center, The First Affiliated Hospital of Dalian Medical University, Dalian 116011, China*

**Wen-Juan Wei** − *Stem Cell Clinical Research Center, The First Affiliated Hospital of Dalian Medical University, Dalian 116011, China*

**Xin Guan** − *Stem Cell Clinical Research Center, The First Affiliated Hospital of Dalian Medical University, Dalian 116011, China*

Complete contact information is available at: https://pubs.acs.org/10.1021/acsomega.1c04894


### Notes

The authors declare no competing financial interest.

## ACKNOWLEDGMENTS

This work was financially supported by the National Natural Science Foundation of China (grant no. 81601202), the Stem Cell Clinical Research Project of China (grant no. CMR-201611-1003), the Liaoning Province Excellent Talent Program (grant no. XLYC1902031), the Dalian Science and Technology Innovation Fund (grant no. 2018J11CY025), and the Dalian Outstanding Young Scholars Program (grant no. 2020RQ077).

## REFERENCES


(1) Lee, D.-H.; Kim, C.-S.; Lee, Y. J. Astaxanthin protects against MPTP/$MPP^+$-induced mitochondrial dysfunction and ROS production *in vivo* and *in vitro*. *Food Chem. Toxicol.* **2011**, *49*, 271−280.

(2) Tian, Y.-Y.; Jiang, B.; An, L.-J.; Bao, Y.-M. Neuroprotective effect of catalpol against $MPP^+$-induced oxidative stress in mesencephalic neurons. *Eur. J. Pharmacol.* **2007**, *568*, 142−148.

(3) Lee, H.-J.; Shin, S. Y.; Choi, C.; Lee, Y. H.; Lee, S.-J. Formation and removal of alphasynuclein aggregates in cells exposed to mitochondrial inhibitors. *J. Biol. Chem.* **2002**, *277*, 5411−5417.

(4) Kalivendi, S. V.; Cunningham, S.; Kotamraju, S.; Joseph, J.; Hillard, C. J.; Kalyanaraman, B. Alpha-synuclein up-regulation and aggregation during MPP+-induced apoptosis in neuroblastoma cells: intermediacy of transferrin receptor iron and hydrogen peroxide. *J. Biol. Chem.* **2004**, *279*, 15240−15247.

(5) Md, S.; Haque, S.; Sahni, J. K.; Baboota, S.; Ali, J. New non-oral drug delivery systems for Parkinson's disease treatment. *Expert Opin. Drug Delivery* **2011**, *8*, 359−374.

(6) Gunay, M. S.; Ozer, A. Y.; Chalon, S. Drug delivery systems for imaging and therapy of Parkinson's Disease. *Curr. Neuropharmacol.* **2016**, *14*, 376−391.

(7) Skibinski, G.; Finkbeiner, S. Drug discovery in Parkinson's disease-Update and developments in the use of cellular models. *Int. J. High Throughput Screening* **2011**, *2011*, 15−25.

(8) Müller, T. Drug therapy in patients with Parkinson's disease. *Transl. Neurodegener.* **2012**, *1*, 10.

(9) Goel, A.; Kunnumakkara, A. B.; Aggarwal, B. B. Curcumin as "Curecumin": from kitchen to clinic. *Biochem. Pharmacol.* **2008**, *75*, 787−809.

(10) Chen, Y.; Lu, Y.; Lee, R. J.; Xiang, G. Nano encapsulated curcumin: and its potential for biomedical applications. *Int. J. Nanomed.* **2020**, *15*, 3099−3120.

(11) Ma, Z.; Wang, N.; He, H.; Tang, X. Pharmaceutical strategies of improving oral systemic bioavailability of curcumin for clinical application. *J. Controlled Release* **2019**, *316*, 359−380.

(12) Heger, M. Don't discount all curcumin trial data. *Nature* **2017**, *543*, 40.

(13) Tapal, A.; Tiku, P. K. Complexation of curcumin with soy protein isolate and its implications on solubility and stability of curcumin. *Food Chem.* **2012**, *130*, 960−965.

(14) Dhule, S. S.; Penfornis, P.; Frazier, T.; Walker, R.; Feldman, J.; Tan, G.; He, J.; Alb, A.; John, V.; Pochampally, R. Curcumin-loaded γ-cyclodextrin liposomal nanoparticles as delivery vehicles for osteosarcoma. *Nanomedicine* **2012**, *8*, 440−451.

(15) Vellampatti, S.; Chandrasekaran, G.; Mitta, S. B.; Lakshmanan, V.-K.; Park, S. H. Metallo-curcumin-conjugated DNA complexes induces preferential prostate cancer cells cytotoxicity and pause growth of bacterial cells. *Sci. Rep.* **2018**, *8*, 14929.

(16) Qi, C.; Wang, D.; Gong, X.; Zhou, Q.; Yue, X.; Li, C.; Li, Z.; Tian, G.; Zhang, B.; Wang, Q.; Wei, X.; Wu, J. Co-delivery of curcumin and capsaicin by dual-targeting liposomes for inhibition of

aHSC-induced drug resistance and metastasis. *ACS Appl. Mater. Interfaces* **2021**, *13*, 16019−16035.
(17) Gong, C.; Deng, S.; Wu, Q.; Xiang, M.; Wei, X.; Li, L.; Gao, X.; Wang, B.; Sun, L.; Chen, Y.; Li, Y.; Liu, L.; Qian, Z.; Wei, Y. Improving antiangiogenesis and anti-tumor activity of curcumin by biodegradable polymeric micelles. *Biomaterials* **2013**, *34*, 1413−1432.
(18) Wu, W.; Shen, J.; Banerjee, P.; Zhou, S. Water-dispersible multifunctional hybrid nanogels for combined curcumin and photothermal therapy. *Biomaterials* **2011**, *32*, 598−609.
(19) Lu, L.; Qi, S.; Chen, Y.; Luo, H.; Huang, S.; Yu, X.; Luo, Q.; Zhang, Z. Targeted immunomodulation of inflammatory monocytes across the blood brain barrier by curcumin-loaded nanoparticles delays the progression of experimental autoimmune encephalomyelitis. *Biomaterials* **2020**, *245*, 119987.
(20) Hettiarachchi, S. S.; Dunuweera, S. P.; Dunuweera, A. N.; Rajapakse, R. M. G. Synthesis of curcumin nanoparticles from raw turmeric rhizome. *ACS Omega* **2021**, *6*, 8246−8252.
(21) Rakotoarisoa, M.; Angelov, B.; Garamus, V. M.; Angelova, A. Curcumin- and fish oil-loaded spongosome and cubosome nanoparticles with neuroprotective potential against $H_2O_2$-induced oxidative stress in differentiated human SH-SY5Y cells. *ACS Omega* **2019**, *4*, 3061−3073.
(22) Rakotoarisoa, M.; Angelova, A. Amphiphilic nanocarrier systems for curcumin delivery in neurodegenerative disorders. *Medicines* **2018**, *5*, 126.
(23) Moghimi, S. M.; Szebeni, J. Stealth liposomes and long circulating nanoparticles: critical issues in pharmacokinetics, opsonization and protein-binding properties. *Prog. Lipid Res.* **2003**, *42*, 463−478.
(24) Immordino, M. L.; Dosio, F.; Cattel, L. Stealth liposomes: review of the basic science, rationale, and clinical applications, existing and potential. *Int. J. Nanomed.* **2006**, *1*, 297−315.
(25) Parodi, A.; Quattrocchi, N.; van de Ven, A. L.; Chiappini, C.; Evangelopoulos, M.; Martinez, J. O.; Brown, B. S.; Khaled, S. Z.; Yazdi, I. K.; Enzo, M. V.; Isenhart, L.; Ferrari, M.; Tasciotti, E. Synthetic nanoparticles functionalized with biomimetic leukocyte membranes possess cell-like functions. *Nat. Nanotechnol.* **2013**, *8*, 61−68.
(26) Wang, C.; Wang, S.; Chen, Y.; Zhao, J.; Han, S.; Zhao, G.; Kang, J.; Liu, Y.; Wang, L.; Wang, X.; Xu, Y.; Wang, S.; Huang, Y.; Wang, J.; Zhao, J. Membrane nanoparticles derived from ACE2-rich cells block SARS-CoV-2 infection. *ACS Nano* **2021**, *15*, 6340−6351.
(27) Zinger, A.; Sushnitha, M.; Naoi, T.; Baudo, G.; De Rosa, E.; Chang, J.; Tasciotti, E.; Taraballi, F. Enhancing inflammation targeting using tunable leukocyte-based biomimetic nanoparticles. *ACS Nano* **2021**, *15*, 6326−6339.
(28) Cocozza, F.; Névo, N.; Piovesana, E.; Lahaye, X.; Buchrieser, J.; Schwartz, O.; Manel, N.; Tkach, M.; Théry, C.; Martin-Jaular, L. Extracellular vesicles containing ACE efficiently prevent infection by SARS-CoV-2 Spike protein-containing virus. *J. Extracell. Vesicles* **2020**, *10*, No. e12050.
(29) Jang, S. C.; Kim, O. Y.; Yoon, C. M.; Choi, D.-S.; Roh, T.-Y.; Park, J.; Nilsson, J.; Lötvall, J.; Kim, Y.-K.; Gho, Y. S. Bioinspired exosome-mimetic nanovesicles for targeted delivery of chemotherapeutics to malignant tumors. *ACS Nano* **2013**, *7*, 7698−7710.
(30) Choo, Y. W.; Kang, M.; Kim, H. Y.; Han, J.; Kang, S.; Lee, J.-R.; Jeong, G.-J.; Kwon, S. P.; Song, S. Y.; Go, S.; Jung, M.; Hong, J.; Kim, B.-S. M1 macrophage-derived nanovesicles potentiate the anticancer efficacy of immune checkpoint inhibitors. *ACS Nano* **2018**, *12*, 8977−8993.
(31) Xuan, M.; Shao, J.; Dai, L.; He, Q.; Li, J. Macrophage cell membrane camouflaged mesoporous silica nanocapsules for *in vivo* cancer therapy. *Adv. Healthcare Mater.* **2015**, *4*, 1645−1652.
(32) Zhang, N.; Song, Y.; Huang, Z.; Chen, J.; Tan, H.; Yang, H.; Fan, M.; Li, Q.; Wang, Q.; Gao, J.; Pang, Z.; Qian, J.; Ge, J. Monocyte mimics improve mesenchymal stem cell-derived extracellular vesicle homing in a mouse MI/RI model. *Biomaterials* **2020**, *255*, 120168.
(33) Blanco, E.; Shen, H.; Ferrari, M. Principles of nanoparticle design for overcoming biological barriers to drug delivery. *Nat. Biotechnol.* **2015**, *33*, 941−951.
(34) Shen, L.-M.; Quan, L.; Liu, J. Tracking exosomes *in vitro* and *in vivo* to elucidate their physiological functions: implications for diagnostic and therapeutic nanocarriers. *ACS Appl. Nano Mater.* **2018**, *1*, 2438−2448.
(35) Yan, F.; Li, L.; Deng, Z.; Jin, Q.; Chen, J.; Yang, W.; Yeh, C.-K.; Wu, J.; Shandas, R.; Liu, X.; Zheng, H. Paclitaxel-liposome-microbubble complexes as ultrasound-triggered therapeutic drug delivery carriers. *J. Controlled Release* **2013**, *166*, 246−255.
(36) Feng, L.; Dou, C.; Xia, Y.; Li, B.; Zhao, M.; Yu, P.; Zheng, Y.; El-Toni, A. M.; Atta, N. F.; Galal, A.; Cheng, Y.; Cai, X.; Wang, Y.; Zhang, F. Neutrophil-like cell-membrane-coated nanozyme therapy for ischemic brain damage and long-term neurological functional recovery. *ACS Nano* **2021**, *15*, 2263−2280.
(37) Xicoy, H.; Wieringa, B.; Martens, G. J. M. The SH-SY5Y cell line in Parkinson's disease research: a systematic review. *Mol. Neurodegener.* **2017**, *12*, 10.
(38) Sun, D.; Zhuang, X.; Xiang, X.; Liu, Y.; Zhang, S.; Liu, C.; Barnes, S.; Grizzle, W.; Miller, D.; Zhang, H.-G. A novel nanoparticle drug delivery system: the anti-inflammatory activity of curcumin is enhanced when encapsulated in exosomes. *Mol. Ther.* **2010**, *18*, 1606−1614.
(39) Kenari, A. N.; Kastaniegaard, K.; Greening, D. W.; Shambrook, M.; Stensballe, A.; Cheng, L.; Hill, A. F. Proteomic and post-translational modification profiling of exosome-mimetic nanovesicles compared to exosomes. *Proteomics* **2019**, *19*, 1800161.


https://doi.org/10.1021/acsomega.1c04894
*ACS Omega* 2021, 6, 32133−32141